# On the rate-dependent properties of open-cell polyurethane foams

Gianpietro Del Piero, Giampiero Pampolini

*Experiments on blocks of open-cell polyurethane foam in uniaxial compression show a progressive strain localization. In a preceding paper, localization is described by a model involving a two-phase nonlinear elastic material. The model is in a good qualitative agreement with experiments, but it was unable to capture some finer aspects of the experimental response, such as stress softening, rate-dependence, and some memory effects. In the context of filler-reinforced rubbers, the inelastic aspects of the response have been studied by several authors. Several models have been proposed, in which a specimen is generally represented as a chain of rheological elements, each consisting of a linear elastic spring set in parallel with one or more dissipative elements. Here we anticipate some results of a research still in progress, in which a good description of the response of open-cell foams is obtained from the existing models for filler-reinforced rubbers by taking visco-elastic dissipative elements obeying a fractional exponential law, and by replacing the convex elastic strain energy of the springs with a non-convex energy of the double-well type.*

## 1 Introduction

Polymeric open-cell foams exhibit a complex non-linear behavior. As shown in Fig. 2, the response curve for uniaxial compression shows three well distinguishable regimes: an initial ascending branch, an almost horizontal plateau, and a second ascending branch. The same three regimes are present at unloading but, instead of following backwards the loading path, the response exhibits a hysteresis loop. Moreover, in the plateau regime a localization of deformation occurs on layers orthogonal to the loading direction, see Fig. 1 and [Lakes et al. (1993); Wang and Cuitinho (2002); Pampolini and Del Piero (2008)].

Many studies, mostly based on numerical simulations, have been addressed to the modeling of macroscopic response in terms of microstructure [Gibson and Ashby (1997); Warren and Kraynik (1997); Laroussi et al. (2002); Gong et al. (2005); Jang et al. (2008)]. Usually, the foam is represented as a periodic structure made of linear elastic beams, and strain localization is attributed to the buckling of the cell ligaments. In the model proposed in [Gioia et al. (2001)] and developed in [Pampolini and Del Piero (2008)], strain localization is attributed to a special non-convex shape of the strain energy density, which is also responsible of the hysteresis loops observed in cyclic tests. This elastic model succeeds in reproducing many general features of the observed response. But it is unable to capture some typical inelastic effects, such as:

- *Rate dependence*, revealed by an increase of the stress with increasing loading rate, see Fig. 2a and the experiments in [Sorrentino et al. (2000)],

- *Stress softening*, that is, a decay of the stress in the subsequent cycles of a cyclic test, see Fig. 2b and the experiments in [White et al. (2000); Deng et al. (2006)],

- *A memory effect*, consisting of a partial stress recovery after a sufficiently long period of rest, see Fig. 3 and the experiments in [White et al. (2000)].

The same effects are present in filled rubbery polymers. In particular, the stress softening observed in these materials is called the Mullins effect [Mullins (1948, 1969); Mullins and Tobin (1957)]. It is generally attributed to the interactions between the polymeric matrix and the fillers [Bueche (1961)], and is regarded as a form of isotropic damage [Ogden and Roxburg (1999); Beatty and Krishnaswamy (2000); Dorfmann and Ogden (2003)].

For polymeric foams, the recovery in time of the loading curves, Fig. 3d, rather suggests that this phenomenon be due to a memory effect. For this reason, we decided to include in the model a rate-dependent dissipation,
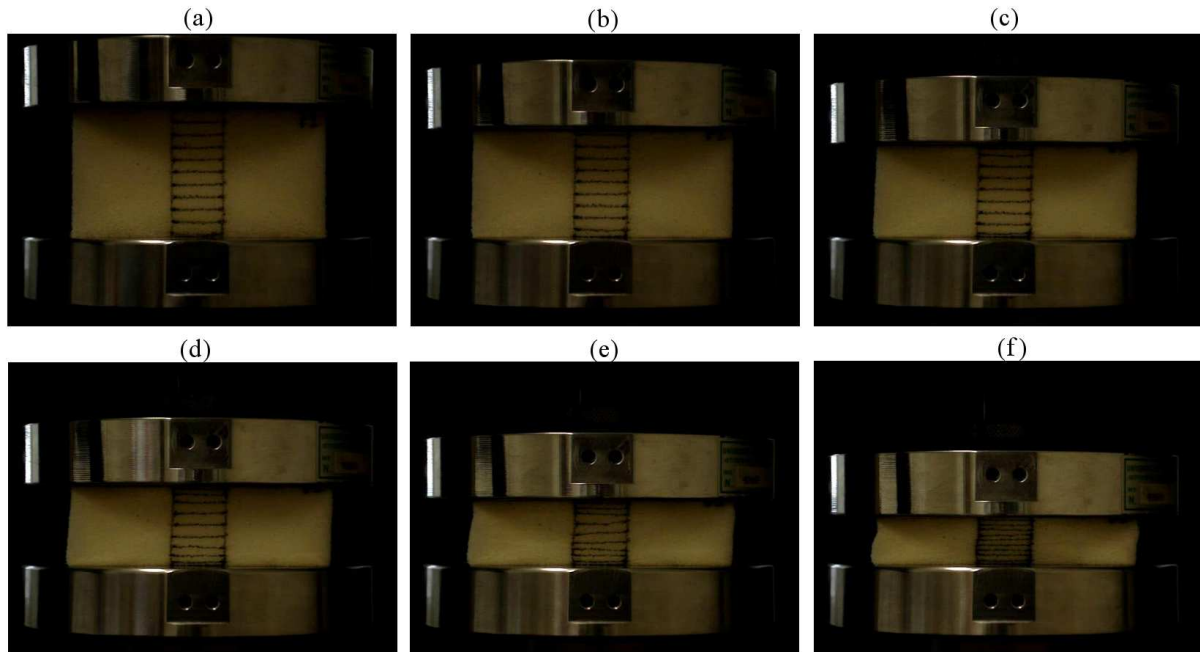
Figure 1: The progressive localization mechanism: the initial homogeneous deformation (a), the first strain localization at the specimens' ends (b), the subsequent propagation to the central layers (c), (d), (e), and the new homogeneous deformation (f).

by introducing visco-elastic damping elements associated with each elastic spring. Here we summarize the first results of our investigation. Throughout this paper, by *stress* we mean the force divided by the initial area, and by *deformation* we mean the ratio between the upper crosshead displacement and the initial distance of the upper crosshead from the fixed lower basis.

## 2  Experiments

The experiments described below were made on a load frame Instron 4467 with a 500 N load cell, located at the Laboratorio di Materiali Polimerici of the University of Ferrara. The specimens were parallelepipeds with base dimensions 100 x 100 mm, cut out from a 50 mm thick sheet of commercial open-cell polyurethane foam. The cutting was done manually, using a ribbon saw. All tests were made at room temperature, controlling the displacement of the upper crosshead, and measuring the force exerted by the sample.

### 2.1  Strain localization

To visualize the phenomenon of strain localization, a rectangular grid has been drawn on one of the specimens' sides. In Fig. 1 the deformation of the grid under uniaxial compression at the constant speed of 5 mm/min is shown. After an initial regime of homogeneous deformation, Fig. 1a, a severe deformation occurred at the specimens' bases, Fig. 1b. This deformation then propagated to the central layers, Fig. 1c,1d, 1e, and finally, after all layers had been reached, the deformation again became homogeneous, Fig. 1f.

### 2.2  Cyclic compression tests

Cyclic compression tests have been performed at the crosshead speeds of 0.1, 5, and 100 mm/min. Three samples were tested for each speed. In all tests, the direction of motion of the crosshead has been reversed when the displacement reached the value of 35 mm, and reversed again at complete unloading, that is, as soon as the load cell measured a null force. Each test consisted of four loading-unloading cycles. The average stress-deformation curves at the first cycle for each of the three speeds are shown in Fig. 2a, while Fig. 2b shows the average curves of the first four cycles for the samples subject to the crosshead speed of 5 mm/min.
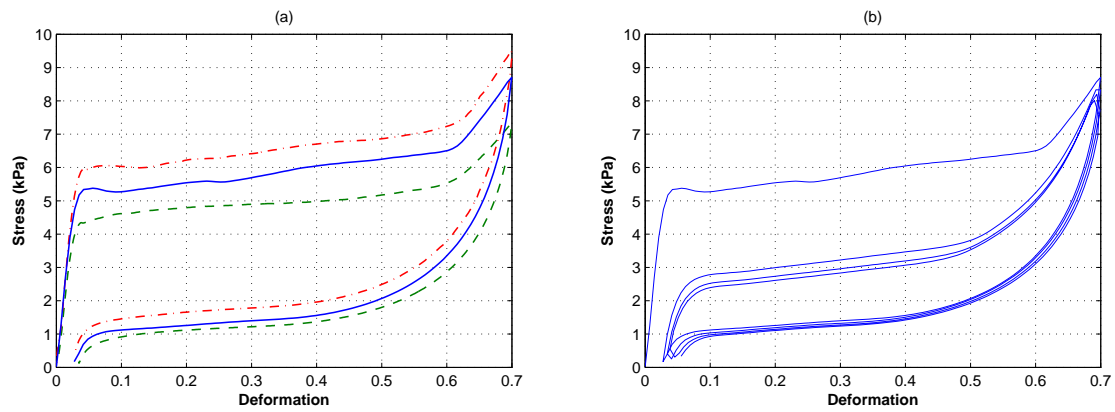
Figure 2: (a) Compression tests at different rates. Force - elongation curves (average on three samples) at crosshead speed of 0.1 mm/min (dashed line), of 5 mm/min (solid line) and of 100 mm/min (dash-dotted line). (b) Cyclic behavior. Cyclic compression test with a crosshead speed of 5 mm/min. Force -elongation curves average on three samples.
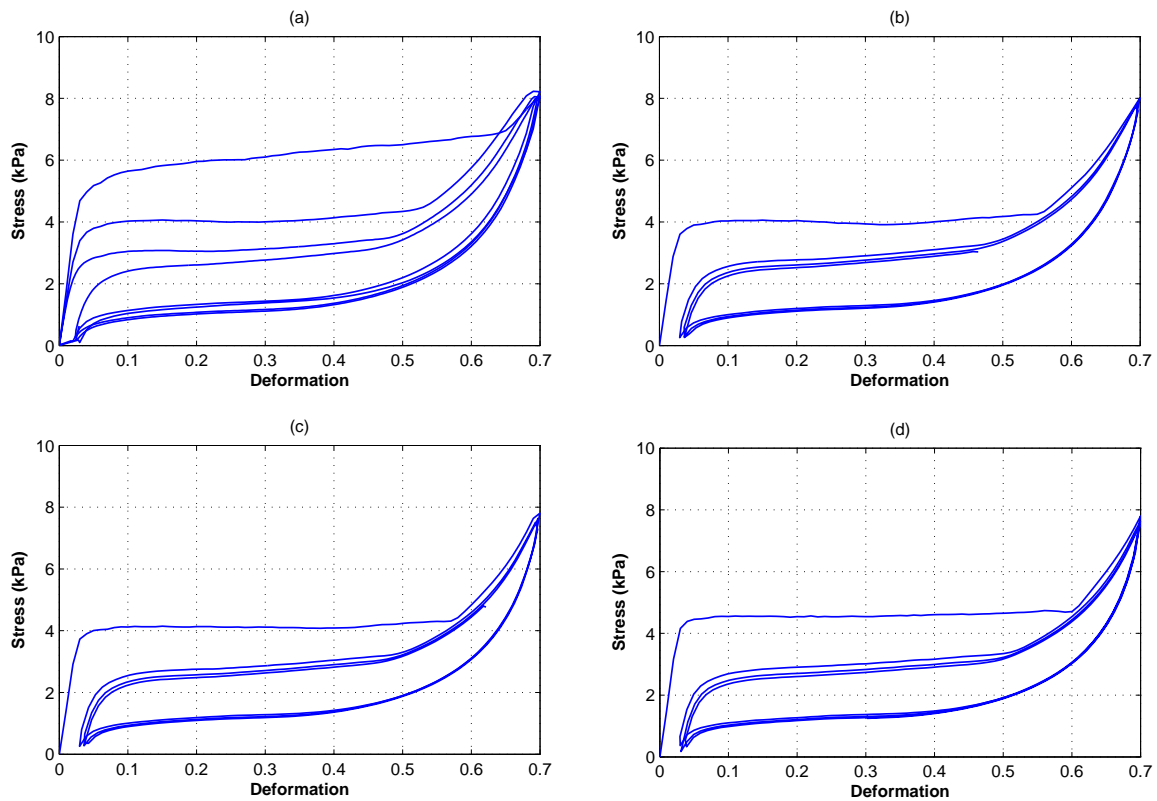


Figure 3: Force-elongation curves in a compression test consisting of four cycles on a virgin sample (a), repeated after three resting periods of 16 hours (b), 52 hours (c) and 33 days (d). Crosshead speed of 5 mm/min.

The first figure shows an overall lifting of the response curves with increasing velocity. The second figure shows the phenomenon of stress softening, which consists of a lowering of the loading curves as the number of cycles increases. The unloading curves remain almost the same for all cycles. Notice that the stress softening is larger between the first and the second cycle, and much less in the subsequent cycles.

Fig. 3 shows the results of an experiment in which a virgin sample was subjected to four cycles of the type described above. The same test was repeated three more times, with resting periods of increasing duration: 16 hours, 52 hours, 33 days. During the resting periods the sample was kept in a box, free of any load and constraint. The four series of response curves are shown in Fig. 3. The first loading curve in the second group is higher than the last loading curve in the first group; in fact, it almost coincides with the second loading curve in the first group. Thus, a significant part of the stress reduction observed at the end of the first group has been recovered after a resting period of 16 hours. In the third test performed after a rest of 52 hours there are no significant changes in the response curves. On the contrary, in the fourth test, after a rest of 33 days, the first loading curve raises of about 10% with respect to the first curve of the preceding test. This stress recovery in time induces us to exclude that the observed stress softening be due to permanent damage.

## 2.3 Loading-unloading cycles in the plateau regime

To investigate the response in the plateau regime we made some cyclic compression tests with small-amplitude loading-unloading cycles. Starting from three different points, located either on the upper or on the lower plateau, we made three cycles of amplitude sufficiently small to avoid phase changes. The force-elongation curves in Fig. 4a and 4b show small hysteresis loops. In a further experiment the loading-unloading cycle was interrupted several times, each time keeping the specimen under constant elongation for a duration of 45 minutes. As shown in Fig. 4c, stress relaxation was observed. This gave us evidence of the presence of viscous effects.
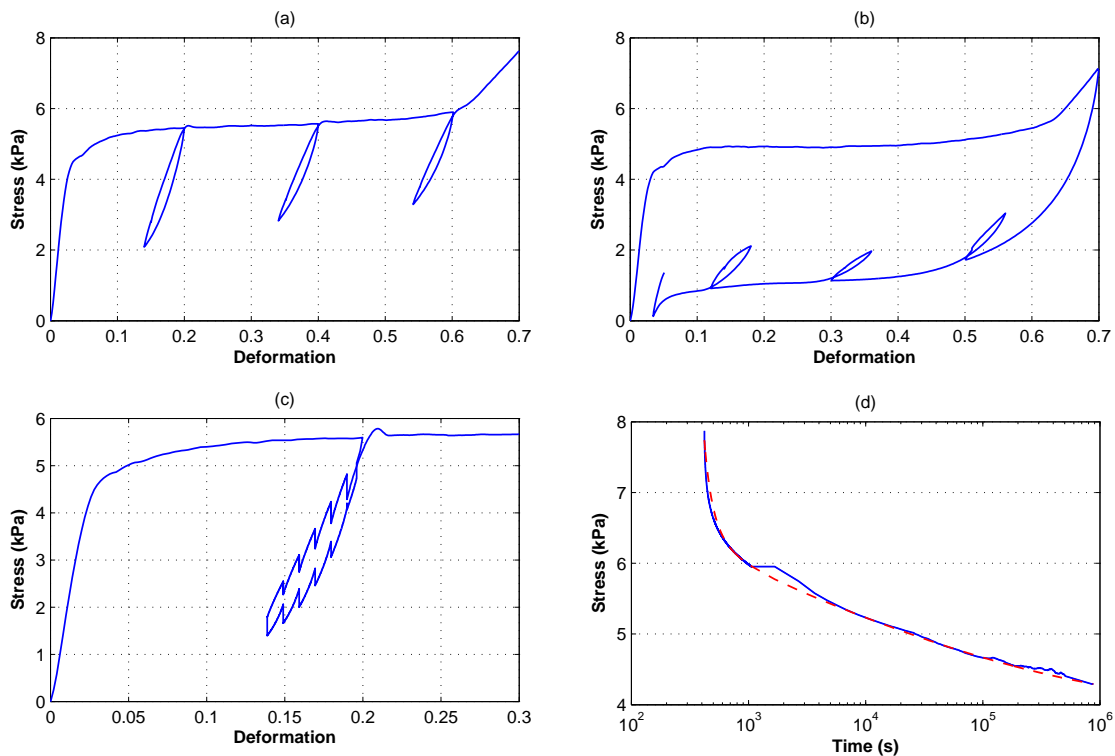


Figure 4: Force-elongation curves for loading-unloading tests inside the hysteresis loop starting from the upper (a) and the lower (b) plateau, and with intermediate rests of 45 min (c). Crosshead speed of 1 mm/min. Relaxation test (d): the experimental curve (full line), and the analytical curve obtained with fractional dashpots (dotted line). The initial part of the experimental curve corresponding to the loading ramp has been omitted. The initial value of the stress is 7.9 kPa.
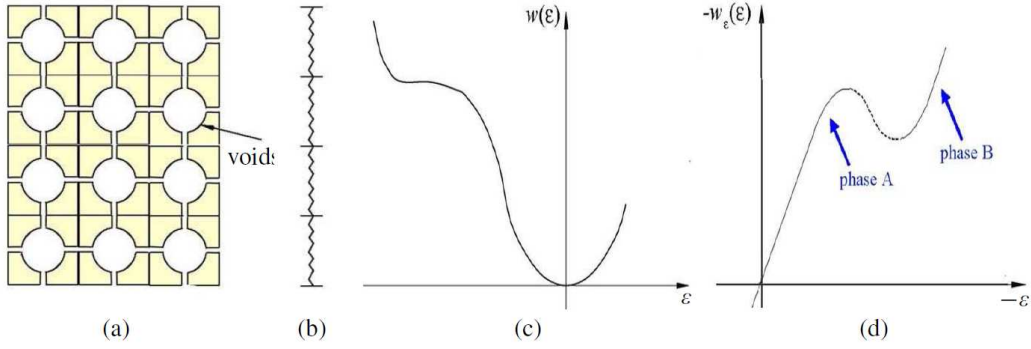
Figure 5: Subdivision of the body into cell layers (a), and representation of each layer as a non linear elastic spring (b) with non convex energy (c), and non-monotonic force-elongation curve (d).

## 2.4 Relaxation tests

To determine the relaxation function of the material, a 10-days relaxation test is performed. A sample is compressed at a crosshead speed of 5 mm/min, till the crosshead displacement reached 35 mm. Then, the upper crosshead is locked and held in position for 10 days. The force is measured at intervals of one second for the first four hours, and then at intervals of 1000 seconds. The stress-time curve is given in Fig. 4d. It shows a very fast initial decay, followed by a long period of slow relaxation. The test was interrupted before the relaxation was complete. Therefore, a full characterization of the relaxation function would need a longer period of observation.

## 3 The elastic model

In the elastic model proposed in [Pampolini and Del Piero (2008)] the foam is modelled as a chain of non-linear elastic springs, in which each spring represents a layer of cells, see Fig. 5. We assume that the energy of a spring only depends on the elongation $\varepsilon$ of the spring, and that all springs have the same energy function $w$. The non-convex form taken for $w$ is shown in Fig. 5c. The corresponding stress-strain curve is shown in Fig. 5d. In it, the two ascending branches form the phases A and B of the material, respectively.

The equilibrium configurations of the chain are identified with the stationary points of the total energy

$$E(\varepsilon_1, \varepsilon_2, \cdots, \varepsilon_N) = \sum_{i=1}^{N} w(\varepsilon_i), \qquad (1)$$

subjected to the hard device condition,

$$\sum_{i=1}^{N} \varepsilon_i = N\varepsilon_0, \qquad (2)$$

where $N\varepsilon_0$ is the given displacement of the upper basis, the displacement at the lower basis being zero.

The stationarity condition requires that the forces $w'(\varepsilon_i)$ transmitted across the springs all have the same value $\sigma$. Moreover, for sufficiently large $N$, a necessary condition for a local energy minimum is that all elongations $\varepsilon_i$ lie on one of the two ascending branches of the stress-strain curve, see [Pampolini and Del Piero (2008)]. Local energy minima correspond to metastable equilibrium configurations. Therefore, a metastable equilibrium configuration may have $M$ springs in phase A and $N - M$ springs in phase B, with $M$ any integer between 0 and $N$.

In Fig. 6a the force-elongation pairs $(\sigma, \varepsilon_0)$ corresponding to metastable equilibrium configurations are shown for a chain made of four springs. We see that they form five ascending curves, the *metastable equilibrium branches*, each corresponding to a value of $M$ between 0 and 4. The stress-free configuration $(\sigma, \varepsilon_0) = (0, 0)$ lies on the equilibrium branch $M = 4$, in which all springs are in phase A. When loaded starting from this configuration, the system follows this branch. The branch ends when $\sigma$ reaches the value $\sigma_{max}$.
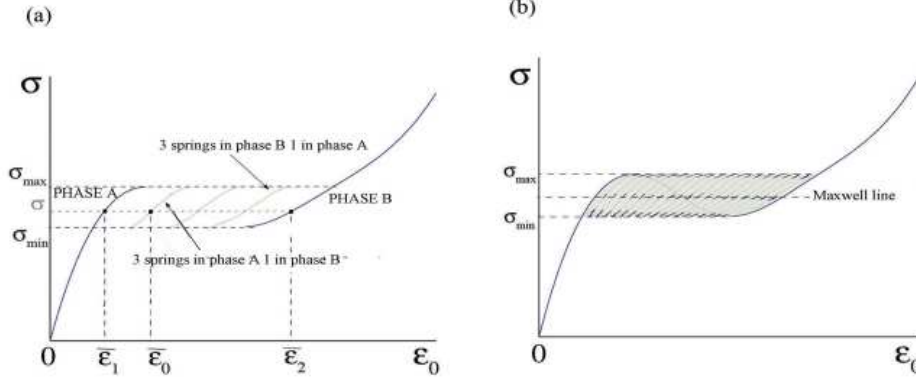
Figure 6: Response curves for a system of 4 springs (a) and for a system of 20 springs (b).

If at this value of $\sigma$ a further elongation is applied, it is reasonable to assume that the system jumps to the metastable branch $M = 3$ with three springs in phase A and one spring in phase B. When this branch ends, the system jumps to the branch $M = 2$, and then to $M = 1$. Finally, it reaches the branch $M = 0$, which corresponds to the single-phase configurations with all springs in phase B.

As shown in Fig. 6b, the amplitudes of the jumps at the end of a branch decreases with increasing $N$. For large $N$, the loading curve becomes a wavy, approximately horizontal line, close to horizontal line $\sigma = \sigma_{max}$. Similarly, the unloading curve becomes close to the line $\sigma = \sigma_{min}$.

This type of response captures some basic aspects of the stress-strain behavior of the material, such as strain localization and hysteresis. Clearly, this purely elastic model cannot capture the inelastic effects. In the next section we take these effects into account, by introducing a visco-elastic dissipative element.

## 4 The visco-elastic model

### 4.1 Discretization in time

Consider a model in which each spring is connected in parallel with a dissipative element, see Fig. 7. This element obeys the linear viscoelastic Boltzmann-Volterra constitutive law

$$\sigma_i^d(t) = \int_0^t G(t-s)\,\dot{\varepsilon}_i(s)\,ds\,, \tag{3}$$

where $\varepsilon_i$ is the elongation of the $i$-th element of the chain, and the relaxation function $G$ is positive and monotonically decreasing. The chain is still subjected to the hard device condition (2), and the force $\sigma_i$ is still the same for all elements. But the force is now the sum of two contributions: an elastic term due to the spring, depending of the current value $\varepsilon_i(t)$, and the visco-elastic term (3), which depends on the whole past history of $\varepsilon_i$:

$$\sigma_i(t) = w'(\varepsilon_i(t)) + \int_0^t G(t-s)\,\dot{\varepsilon}_i(s)\,ds \qquad i = 1, 2, \ldots N\,. \tag{4}$$

For a given loading process $t \mapsto \varepsilon(t)$, we have to solve the problem of finding the force $\sigma(t)$ and the elongations $\varepsilon_i(t)$ which satisfy equations (2) and (4) for all $t$, under given initial conditions $\varepsilon_i(0) = \varepsilon_{i0}$. The problem admits the homogeneous solution $\varepsilon_i(t) = \varepsilon(t)$. This solution is unique if $G$ is positive and monotonically decreasing and $w$ is convex, see [Del Piero and Pampolini (2009)]. If $w$ is non-convex, non-homogeneous solutions may exist. They can be approximately determined via time discretization. Using the incremental approach described in [Del Piero and Pampolini (2009)], the incremental version of equations (4)

$$\dot{\sigma} - Q_i(t)\dot{\varepsilon}_i = A_i(t)\,, \tag{5}$$

is obtained, where

$$Q_i(t) \doteq w''(\varepsilon_i(t)) + G(0)\,, \qquad A_i(t) \doteq \int_0^t \dot{G}(t-s)\,\dot{\varepsilon}_i(s)\,ds\,. \tag{6}$$
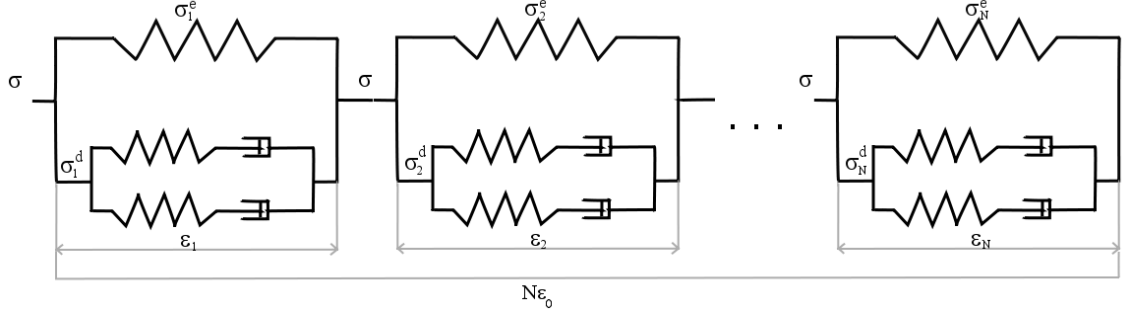
Figure 7: The visco-elastic model.

These equations, together with the incremental version of (2)

$$\sum_{i=1}^{N} \dot{\varepsilon}_i(t) = N\dot{\varepsilon}(t)\,, \tag{7}$$

provide, for each $t$, a system of $N+1$ linear algebraic equations for the unknowns $\dot{\sigma}(t), \dot{\varepsilon}_i(t)$.

The system has a unique solution if all coefficients $Q_i$ are different from zero. If only one coefficient vanishes, $Q_N = 0$, in analogy with what is made for the elastic model, we assume that the $N$-th element undergoes a phase change. If more than one coefficients vanish, the system admits a multiplicity of solutions. In this case, uniqueness is recovered assuming that only one element undergoes a phase change [Del Piero and Pampolini (2009)].

In the present dissipative context, the concept of *phase* needs to be suitably re-defined. Assume that the function $w''$ is concave. Then the set of all $\varepsilon$ for which $w''(\varepsilon) + G(0) < 0$ is an interval $(\varepsilon_A, \varepsilon_B)$. We say that the $i$-th element is in phase A at time $t$ if $\varepsilon_i(t) \leq \varepsilon_A$, and that it is in phase B if $\varepsilon_i(t) \geq \varepsilon_B$. Notice that, because $G(0) > 0$, the interval $(\varepsilon_A, \varepsilon_B)$ is strictly contained in the interval which separates the two phases in the absence of viscous dissipation.

A change of phase still consists in the jump of one of the elastic springs from one phase to the other. At a fixed time $t$, suppose that the first $M$ elements are in phase A and the remaining $N-M$ are in phase B. Also assume that $Q_M(t) = 0$ and that, under a given increment $\delta_\varepsilon$ of the total elongation, the $M$-th element undergoes the transition from phase A to phase B.

The increments $\delta_i, \delta_\sigma$, of $\varepsilon_i, \sigma$, occurring during the phase change are determined by the $N+1$ algebraic equations

$$
\begin{aligned}
&\sum_{i=1}^{N} \delta_i = \delta_\varepsilon\,, \\
&w_A'(\varepsilon_i(t) + \delta_i) + B_i(t) + G_\tau\,\delta_i = \delta_\sigma \quad \forall i \in \{1, \ldots M-1\}\,, \\
&w_B'(\varepsilon_M(t) + \delta_M) + B_M(t) + G_\tau\,\delta_M = \delta_\sigma\,, \\
&w_B'(\varepsilon_i(t) + \delta_i) + B_i(t) + G_\tau\,\delta_i = \delta_\sigma \quad \forall i \in \{M+1, \ldots N\}\,,
\end{aligned}
\tag{8}
$$

where

$$B_i(t) \doteq -w_A'(\varepsilon_i(t)) + \int_0^t \big(G(t+\tau - s) - G(t-s)\big)\,\dot{\varepsilon}_i(s)\,ds\,, \tag{9}$$

and $w_A$ and $w_B$ are the restrictions of $w$ to $(0, \varepsilon_A)$ and to $(\varepsilon_B, +\infty)$, respectively.

## 4.2 Characterization of the material parameters

For the spring we take the non-convex double-well strain energy [Pampolini and Del Piero (2008)]

$$
\begin{aligned}
w(\varepsilon_i) = {}& \frac{1}{2}\,\gamma\,(1+\varepsilon_i)^2 + c\,(1+\varepsilon_i)^m \Big(\frac{1}{m+2}\,(1+\varepsilon_i)^2 - \frac{1}{m}\Big) \\
& - \mu \log(1+\varepsilon_i) + \frac{\beta\sqrt{\pi}}{2\sqrt{k}}\,\mathrm{erf}\big(\sqrt{k}(\varepsilon_i - \zeta)\big) + \delta\,,
\end{aligned}
\tag{10}
$$

where $\mathrm{erf}\,(\cdot)$ is the error function

$$\mathrm{erf}(x) = \frac{2}{\sqrt{\pi}}\int_0^x \exp(-t^2)\,dt\,, \tag{11}$$

Table 1: The values of the material constants used in the numerical simulations.

| $c$ | $m$ | $\mu$ | $\zeta$ | $\beta$ | $k$ |
|-----|-----|-------|---------|---------|-----|
| 70 kPa | 12 | 1 kPa | 0.8 | 0.5 kPa | 160 |

| $K_1$ | $r_1$ | $\eta_1$ | $K_2$ | $r_2$ | $\eta_2$ |
|-------|-------|----------|-------|-------|----------|
| 4.5 kPa | 0.32 s | $4.5\,10^4$ kPa s | 12.72 kPa | 0.89 | 763.2 kPa s |

$c, m, \mu, \beta, k, \zeta$ are positive constants, and $\gamma, \delta$ are constants whose values

$$
\gamma = \mu - \beta \exp(-k\zeta^2),
$$
$$
\delta = -\frac{1}{2}(\mu - \beta \exp(-k\zeta^2)) + \frac{2c}{m(m+2)} - \frac{\beta\sqrt{\pi}}{2\sqrt{k}}\,\mathrm{erf}(\sqrt{k}\,\zeta)\,,
\tag{12}
$$

are such that both the force and the strain energy are zero at the reference configuration $\varepsilon_i = 0$. The values taken for the remaining elastic constants are given in Table 1. The force in the spring

$$
\sigma_i^e(\varepsilon_i) = (1 + \varepsilon_i)\big(\mu - \beta \exp(-k\,\zeta^2)\big) + c\,(1 + \varepsilon_i)^{m-1}((1 + \varepsilon_i)^2 - 1)
$$
$$
-\mu\,(1 + \varepsilon_i)^{-1} + \beta \exp(-k(\varepsilon_i - \zeta)^2)
\tag{13}
$$

is obtained by differentiation of the energy.

As shown in Fig. 4d, the relaxation function is characterized by two well distinct regimes: a fast stress decay of the duration of a few seconds, followed by a regime of slow decay whose duration exceeds the ten days of the duration of the test. The same figure shows that the relaxation curve is conveniently approximated by the two fractional Maxwell elements connected in parallel represented in Fig. 7. Each element is formed by a linear elastic spring of stiffness $K_{i\alpha}$ and by a dashpot obeying the laws

$$
\sigma_{i\alpha}(t) = K_{i\alpha}\varepsilon_{i\alpha}^e(t)\,, \quad \sigma_{i\alpha}(t) = \eta_\alpha \frac{d^{r_\alpha}}{dt^{r_\alpha}}\varepsilon_{i\alpha}^d(t)\,, \quad i = 1, \ldots N, \ \ \alpha = 1, 2,
\tag{14}
$$

respectively, where $\varepsilon_{i\alpha}^e$, $\varepsilon_{i\alpha}^d$, are the elongations of the $\alpha$-th spring and dashpot, respectively, of the $i$-th element, $\eta_\alpha$ are positive constants, and $r_\alpha$ are numbers between 0 and 1. For $r_\alpha = 1$ the fractional derivative reduces to the ordinary derivative, see [Koeller (1984); Gorenflo and Mainardi (1997)] for details. The force $\sigma_i^d$ acting on the whole element is the sum of the forces $\sigma_{i\alpha}$ acting in the dashpots

$$
\sigma_i^d(t) = \sum_{\alpha=1}^{2} \eta_\alpha \frac{d^{r_\alpha}}{dt^{r_\alpha}}\varepsilon_{i\alpha}^d(t)\,.
\tag{15}
$$

This equation is a special case of the Boltzmann-Volterra constitutive law (3), obtained from the relaxation function

$$
G(t) = \sum_{\alpha=1}^{2} K_\alpha\, E_{r_\alpha}\!\left(-\left(\frac{K_\alpha t}{\eta_\alpha}\right)^{r_\alpha}\right)\,,
\tag{16}
$$

where $E_{r_\alpha}(\cdot)$ is the Mittag-Leffler function

$$
E_{r_\alpha}(x) = \sum_{n=0}^{\infty} \frac{x^n}{\Gamma(r_\alpha n + 1)}\,,
\tag{17}
$$

with $\Gamma(\cdot)$ the Gamma function, see [Koeller (1984); Lion (1997)]. The parameters $K_\alpha, \eta_\alpha$ and $r_\alpha$ were calibrated to obtain an optimal representation of the experimental relaxation curve, see Fig. 4d. Their values are reported in Table 1.

### 4.3 Numerical simulations

To find the response to a loading process $t \to \varepsilon(t)$ we take time intervals $(t_n, t_{n+1})$, $n = 1, 2, \ldots$, and approximating functions with time derivatives constant in each interval. If the solution at time $t_n$ is known and if all coefficients $Q_i(t_n)$ are positive, the solution at time $t_{n+1}$ can be computed by solving the system of equations (5) and (7), with the solution of the preceding step as initial condition. If at time $t_n$ one or more coefficients $Q_i(t_n)$
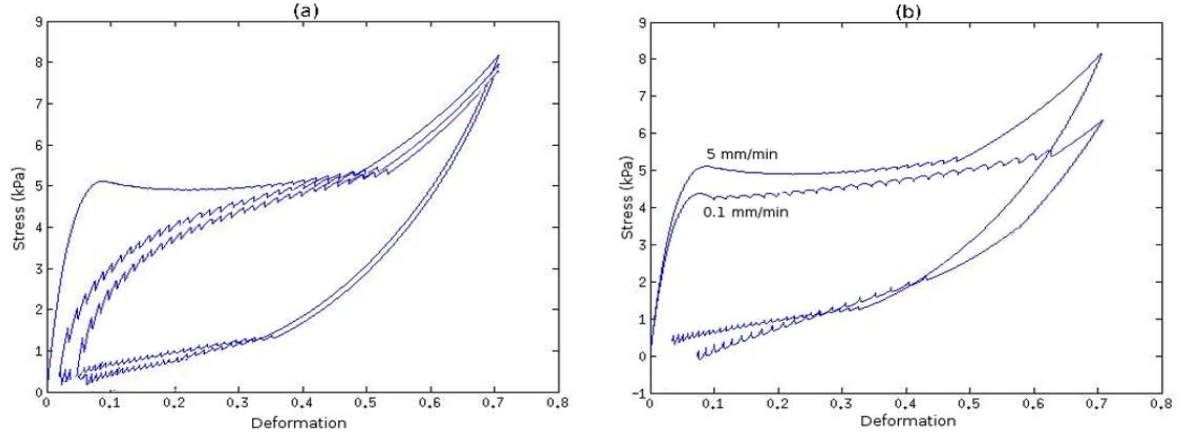
Figure 8: Numerical simulations for a chain of 30 elements in a cyclic test at 5 mm/min (a), and in a simple loading-unloading test at two different rates (b).
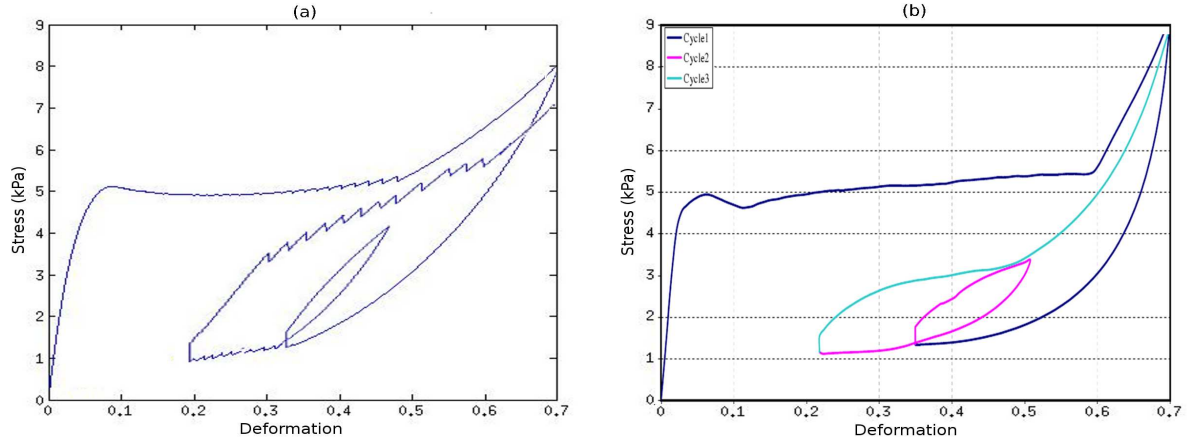


Figure 9: Comparison between the experiments (right), and the prediction of the proposed model (left) for a complex loading unloading process.

are non-positive a change of phase occurs, and the solution is calculated by solving the system (8). In our computations, this has been done with an iterative method based on the Newton-Raphson procedure. The numerical experiments are still in progress, and only partial results are available at the moment. Fig. 8a shows a simulation of the stress softening phenomenon, obtained with a chain of 30 elements and assuming a loading rate of 5 mm/min. The main general features of the simulated response are:

- the lowering of the loading curve with increasing number of cycles,

- a sharp transition from the first ascending branch to the plateau in the first cycle, and a more gradual transition in the following cycles,

- a substantial independence of the unloading curves on the number of cycles,

- a residual deformation at the end of each cycle.

Comparing the results with the experimental curves of Fig. 2b, one may see some discrepancies:

- In the numerical simulation, the transition between the plateau regime and the second ascending branch occurs at a deformation which does not significally change with the number of cycles. In the experiments, one has $\varepsilon = 0.6$ at the first cycle and $\varepsilon = 0.5$ at the subsequents cycles.

- In the simulation, the slope of the plateau increases with the number of cyles. In the experimental curves, the slope of the plateau is essentially the same for all cycles.

82

These discrepancies can be attributed to an insufficient number $N$ of elements. Indeed, in the simulation there are jumps at the phase changes in all cycles after the first, while the experimental response is smooth. In the elastic model the jump amplitudes tend to zero with increasing $N$, see Fig. 6. An investigation on the influence of the number of the elements in the visco-elastic model is now in progress.

In Fig. 8b are shown the simulations of a single loading-unloading cycle at two different loading rates, 5 and 0.1 mm/min. One sees a lifting of the response curve with increasing loading rate, more evident at loading than at unloading. This is in agreement with experiments. On the contrary, there is no experimental confirmation of the different length of the plateau predicted by the two simulations.

A simulation of a complex loading-unloading process is shown in Fig. 9. We see that the model gives a qualitative description of the behavior of the foam, including the small hysteresis loop from the lower plateau and the small vertical segments $\varepsilon = 0.35$ and $\varepsilon = 0.22$ at the end of the two unloading curves, which are due to some period of rest before reloading.

The third loading curve in the simulation is not quite satisfactory. Instead of being smooth, it presents some evident jumps. Moreover, it does not reach the same force level reached at first loading, as it occurs in the experimental curve. Simulations with larger $N$ may reduce these dicrepancies.

## References

Beatty, M.; Krishnaswamy, S.: A theory of stress-softening in incompressible isotropic materials. *J. Mech. Phys. Solids*, 48, (2000), 1931–1965.

Bueche, F.: Mullins effect and rubber-filler interaction. *J. Appl. Polymer Sci.*, 15, (1961), 271–281.

Del Piero, G.; Pampolini, G.: On the inelastic properties of open-cell polymeric foams: experiments and theoretical model. *in preparation.*

Deng, R.; Davies, P.; Bajaj, A.: A nonlinear fractional derivative model for large uni-axial deformation behavior of polyurethane foam. *Signal Processing*, 86, (2006), 2728–2743.

Dorfmann, A.; Ogden, R. W.: A pseudo-elastic model for loading, partial unloading and reloading of particle-reinforced rubber. *Int. J. Solids Struct.*, 40, (2003), 2699–2714.

Gibson, L. J.; Ashby, M. F.: *Cellular Solids: Structure and Properties*. Cambridge University Press, second edn. (1997).

Gioia G.; Wang Y,; Cuitiño A.M,: The energetics of heterogeneous deformation in open-cell solid foams. *Proc. R. Soc. London A* 457, (2001) 1079–1096.

Gong, L.; Kyriakides, S.; Jang, W. Y.: Compressive response of open-cell foams. Part I: Morphology and elastic properties. *Int. J. Solids Struct.*, 42, (2005), 1355–1379.

Gorenflo, R.; Mainardi, F.: *Fractional calculus: integral and differential equations of fractional order*. In: Carpinteri A.; Mainardi F. eds.: *Fractals and fractional calculus in continuum mechanics*, CISM Courses and Lectures, 378. Springer (1997).

Jang W.-Y.; Kraynik, A M.; Kyriakides, S.: On the microstructure of open-cell foams and its effect on elastic properties. *Int. J. Solids Struct.*, 45, (2008), 1845–1875.

Koeller, R. C.: Applications of fractional calculus to the theory of viscoelasticity. *Journal of Applied Mech.*, 51, (1984), 299–307.

Lakes, R.; Rosakis, P.; Ruina, A.: Microbuckling instability in elastomeric cellular solids. *J. Mater. Sci.*, 28, (1993), 4667–4672.

Laroussi, M.; Sab, K.; Alaoui, A.: Foam mechanics: nonlinear response of an elastic 3d-periodic microstructure. *Int. J. Solids Struct.*, 39, (2002.), 3599–3623.

Lion, A.: On the thermodynamics of fractional damping elements. *Cont. Mech. Thermodyn.*, 9, (1997), 83–96.

Mullins, L.: Effect of stretching on the properties of rubber. *Rubber Chem. Technol.*, 21, (1948), 281–300.

Mullins, L.: Softening of rubber by deformation. *Rubber Chem. Technol.*, 42, (1969), 339–362.

Mullins, L.; Tobin, N.: Theoretical model for the elastic behavior of filler-reinforced vulcanized rubbers. *Rubber Chem. Technol.*, 30, (1957), 555–571.

Ogden, R. W.; Roxburg, D. G.: A pseudo-elastic model for the mullins effect in filled rubber. *Proc. R. Soc. London A*, 455, (1999), 2861–2877.

Pampolini, G.; Del Piero, G.: Strain localization in open-cell polyurethane foams: experiments and theoretical model. *Journal Mech. Materials Struct.*, 3, (2008), 969–981.

Sorrentino, L.; Aurelia, M.; Iannace, S.: A simple method to predict high strain rates mechanical behavior of low interconnected cell foams. *Polymer Testing*, 26, (2000), 878–885.

Wang, Y.; Cuitinho, A. M.: Full-field measurements of heterogeneous deformation patterns on polymeric foams using digital image correlation. *Int. J. Solids Struct.*, 39, (2002), 3777–3796.

Warren, W. E.; Kraynik, A. M.: Linear elastic behavior of a low-density Kelvin foam with open cells. *ASME J. Appl. Mech.*, 64, (1997), 787–793.

White, S. W.; Kim, S. K.; Bajaj, A. K.; Davis., P.: Experimental techniques and identification of nonlinear and viscoelastic properties of flexible polyurethane foam. *Nonlinear Dynamics*, 22, (2000), 281–313.

---

*Addresses:* Gianpietro Del Piero, Università di Ferrara, Via Saragat 1, 44100 Ferrara, Italy
Giampiero Pampolini, C.N.R.S., Laboratoire de Mécanique et d'Acoustique, 31 Chemin Joseph Aiguier, 13402 Marseille, France.
email: `dlpgpt@unife.it`, `pampolini@lma.cnrs-mrs.fr`.